Cell

Specified Neural Progenitors Sort to Form Sharp Domains after Noisy Shh Signaling

Fengzhu Xiong,[1] Andrea R. Tentner,[1] Peng Huang,[2] Arnaud Gelas,[1] Kishore R. Mosaliganti,[1] Lydie Souhait,[1] Nicolas Rannou,[1] Ian A. Swinburne,[1] Nikolaus D. Obholzer,[1] Paul D. Cowgill,[1] Alexander F. Schier,[2] and Sean G. Megason[1,*]

[1]Department of Systems Biology, Harvard Medical School, Boston, MA 02115, USA

[2]Department of Molecular and Cellular Biology, Center for Brain Science, Harvard Stem Cell Institute, Broad Institute, Harvard University, Cambridge, MA 02138, USA

*Correspondence: megason@hms.harvard.edu

http://dx.doi.org/10.1016/j.cell.2013.03.023

SUMMARY

Sharply delineated domains of cell types arise in developing tissues under instruction of inductive signal (morphogen) gradients, which specify distinct cell fates at different signal levels. The translation of a morphogen gradient into discrete spatial domains relies on precise signal responses at stable cell positions. However, cells in developing tissues undergoing morphogenesis and proliferation often experience complex movements, which may affect their morphogen exposure, specification, and positioning. How is a clear pattern achieved with cells moving around? Using in toto imaging of the zebrafish neural tube, we analyzed specification patterns and movement trajectories of neural progenitors. We found that specified progenitors of different fates are spatially mixed following heterogeneous Sonic Hedgehog signaling responses. Cell sorting then rearranges them into sharply bordered domains. Ectopically induced motor neuron progenitors also robustly sort to correct locations. Our results reveal that cell sorting acts to correct imprecision of spatial patterning by noisy inductive signals.

INTRODUCTION

Two central questions in developmental biology are how cell-type diversity is generated and how these types are organized into patterns of structural and functional significance. The classic "French flag" model (Wolpert, 1969) put forward the idea of morphogen patterning that mechanistically couples specification and spatial arrangement. In this view, a gradient of a diffusible signal across a field of naive cells defines spatial domains of cell types between concentration thresholds. Recent studies have challenged and extended this model in several aspects. First, a signaling gradient may not be sufficient to generate precise cell-type boundaries, given the noise inherent in molecular processes and the limited information content of gradients in vivo (Paulsson, 2004; Lander et al., 2009). Second, the timing of exposure to the signal, in addition to concentration, contributes to cell fate choices (Ahn and Joyner, 2004; Harfe et al., 2004; Dessaud et al., 2007). Third, the position of a cell relative to a morphogen source may change in time through cell migration and division (Kay and Thompson, 2009). Fourth, lateral cell-cell interactions such as cell sorting may also be involved in boundary formation (Lawrence et al., 1999; Nicol et al., 1999; Xu et al., 1999).

A prominent example of morphogen patterning is the vertebrate ventral neural tube. In this system, sharply bordered progenitor domains form along the ventral-dorsal axis (Jessell, 2000; Figure S1A available online). This spatial arrangement is important for the localization, migration, and wiring of neurons born from these domains (Lewis and Eisen, 2003; Sürmeli et al., 2011). Significant molecular insights have been generated toward the understanding of how this pattern forms. First, the secreted signaling protein Sonic Hedgehog (Shh) is produced in the notochord underlying the neural tube and later in the floor plate (Krauss et al., 1993; Echelard et al., 1993) and likely forms a ventral-to-dorsal gradient in the neural tube (Yamada et al., 1993; Chamberlain et al., 2008). Second, gene expression induced by different Shh signaling levels as a function of concentration and duration of exposure in vitro parallels the spatial ordering of the expression domains of the same genes in vivo (Ericson et al., 1997; Dessaud et al., 2007). Third, intracellular gene regulatory network (GRN) interactions between Shh-regulated transcription factors establish stable and discrete fates that no longer depend on Shh (Lek et al., 2010; Balaskas et al., 2012). Together, these studies provide the molecular scenario of morphogen patterning in the neural tube: each cell measures its Shh exposure and enters a corresponding state of gene expression; the states dynamically evolve under the GRN to become self-sustaining, mutually exclusive, and cell-type specific; the Shh gradient is thus translated into discrete progenitor domains. In this model, the shape of the morphogen gradient in time and space is directly predictive of the final pattern. Therefore, for the sharply bordered spatial domains in the neural tube to form, Shh exposure levels as a function of position and

time must be precise, especially at the putative domain boundaries. In addition, cells should maintain stable positions relative to the source of Shh to receive a correct signal input over time. It is unclear whether these requirements for low signaling and positional noise are found in vivo or whether additional mechanisms are required to ensure the precision of patterning.

The dynamics of cell movements might provide an answer to these questions. The transition of the neural plate to the neural tube involves extensive cell migration, intercalation, and proliferation (Schoenwolf, 1991; Kimmel et al., 1994; Ciruna et al., 2006) that take place concurrently with Shh gradient formation and interpretation (Martí et al., 1995; Takamiya and Campos-Ortega, 2006). Studies using clonal labeling show cell mixing during morphogenesis and after divisions to variable degrees in the neural tubes of different vertebrates (Leber and Sanes, 1995; Erskine et al., 1998; Inoue et al., 2000; Park et al., 2004), depending on the developmental stage and the anterior-posterior (AP) level. These cellular positional dynamics may affect patterning in several ways. First, movement of Shh-producing and -responding cells may alter the spatial distribution of Shh ligands among the progenitors, affecting the morphogen gradient. Second, movement of an unspecified progenitor in the gradient may cause its Shh exposure level to change over time, potentially affecting its fate decision (Dessaud et al., 2007). Third, movement of specified progenitors may either disrupt or sharpen domain boundaries. To evaluate these possibilities, it is essential to understand how individual progenitors behave throughout patterning, proliferation, and morphogenesis.

Here, we use in toto imaging to fully capture ventral neural tube formation with single-cell resolution in living zebrafish embryos and report systematic cell-tracking analysis of the movies. Our results reveal that intensive cell movements accompany patterning. Shh-responding cells show spatial heterogeneity of signaling and become specified to different ventral fates in intermingled distributions. Surprisingly, they then sort out into sharply bordered domains in a robust and Shh-independent manner to make the final pattern. Cadherin-mediated cell adhesion is required for the sorting process. These data support a revised French flag model where pattern formation in the neural tube is achieved by sorting of specified cells following noisy morphogen-based specification.

RESULTS

In Toto Imaging Reveals Cell Dynamics during Neural Tube Patterning in Zebrafish

The lack of understanding of neural progenitor movements is mainly due to the unavailability of live-cell tracking data. Direct imaging of the neural plate is challenging because it undergoes drastic morphogenetic movements, including transition of a horizontal lateral-medial (LM) axis to the vertical dorsal-ventral (DV) axis, morphological and polarity changes of cells, and frequent cell divisions (Clarke, 2009). We designed an in toto imaging (Megason and Fraser, 2003) system in zebrafish embryos, whose fast development, small size, and transparency make full-coverage live imaging feasible. Using an immersed dorsal mount, we allow unrestricted morphogenesis while the embryo sits stably in the field of view (Figures 1A and S1B). This enables uninterrupted imaging sessions on single embryos from early neural plate to neural tube stages using confocal/two-photon microscopy. We acquired high-resolution image stacks every 2–3 min of healthy embryos labeled with nuclear/membrane fluorescent proteins and transgenic reporters (Figures 1B, S1B, S1C, and S1E; data not shown). These data provide trackable movies of ventral neural tube formation (Movie S1). They thoroughly cover the period of Shh expression, progenitor responses, and the establishment of stable pattern (Figure 1D, i; Krauss et al., 1993; Huang et al., 2012), allowing us to directly watch patterning (Figure 1E; Movie S2). We manually tracked cells using the GoFigure 2 software that we have developed (Figures 1C and S1D; Extended Experimental Procedures). These tracks provide systematic and quantitative data on transgenic reporter expression (Figure 1D, ii), lineage relationships (Figure 1D, iii), and, importantly, positional dynamics (Figure 1D, iv) of the neural progenitors, allowing us to study the role of cell movements in pattern formation.

To assess the extent of cell movement, we calculated progenitor speeds at different times (Figures 1F and S1F). Cells show extensive movements that slow down gradually on the population level as the neural tube forms between 10 and 16 hr postfertilization (hpf). For individual cells, mobility is reduced when they become epithelialized (Movie S3; data not shown). These data indicate that patterning occurs at a time when cells are moving, on average at a fast rate of one cell diameter every 10–20 min, not when the field of cells is static. It is intriguing that sharp spatial domains arise correctly in such a dynamic environment.

Shh-Expressing and -Responding Cells Show Dynamic Movements and Heterogeneous Levels

To characterize how patterns of Shh signaling may change during the cell movements, we first imaged Shh reporter *tg(shh:gfp)* (Shkumatava et al., 2004) embryos to follow Shh-producing cells (Figure 2A). Shh expression begins early during epiboly, before there is a notochord or neural tube (Krauss et al., 1993). At this stage, prenotochord axial mesoderm cells form a wide *shh:gfp*+ plate underneath the neural ectoderm, rendering more than ten future neural plate cells in cross-section as direct neighbors to Shh-producing cells. This arrangement changes drastically as the notochord condenses and medial floor plate (MFP) cells start to express Shh, until finally only two GFP− neural tube cells directly border Shh-producing cells (MFPs).

These dynamic movements of source cells may generate a spatially and temporally changing Shh signaling profile. For example, cells might receive less Shh after moving away from Shh-producing cells that are initially their neighbors. To explore this idea, we imaged *tgBAC(ptch2:kaede)* (Huang et al., 2012) embryos that report the level of Shh signaling in responding cells (Figures 2B and S1A). Interestingly, at 10 hpf, neighbor cells at the same location often have very different Kaede levels, and some Kaede+ cells can be found at large distances from the notochord resulting in a highly heterogeneous spatial response distribution (Figure 2B, i and ii). The heterogeneity persists as the neural keel forms (12 hpf; Movie S4), and lasts until 14.5 hpf, at which time a clear and sharp gradient can be seen corresponding to different stereotypic cell-type locations (Figure 2B, iii and iv, and Movie S4). To compare Shh spatial responses

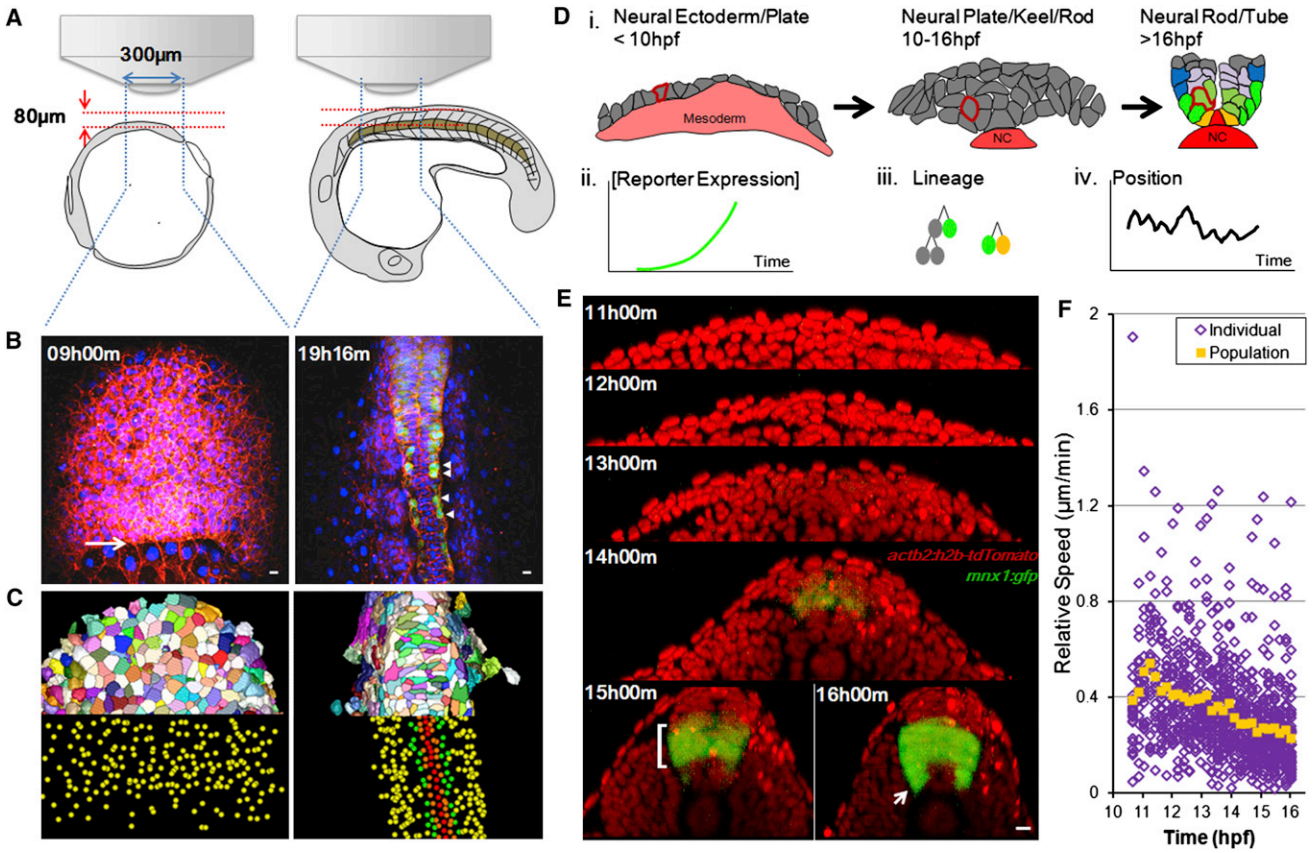

Figure 1. In Toto Imaging Captures Dynamics of Neural Progenitors during Neural Tube Formation in Zebrafish Embryos

(A) Schematic illustration of imaging setup. See also the Extended Experimental Procedures.

(B) Sample time points of raw data rendered in 3D projection dorsal view. Red indicates mem-citrine, blue designates h2b-cherry, and green shows *mnx1:gfp*. Arrow points to the frontier of epiboly movement. Arrowheads indicate differentiating MNs. All time annotations are hours (and minutes) postfertilization (hpf). Scale bars, 10 μm. See also Movie S1.

(C) Processed data by GoFigure 2 and ACME (Mosaliganti et al., 2012) software from images in (B). Top halves: membrane segmentations (random colors to distinguish neighbors); bottom halves: nuclei segmentations for cell tracking (red indicates MFPs, orange indicates LFPs, green shows pMNs, and yellow indicates unidentified cells).

(D) Schematic illustration of cell-tracking analysis. Drawings are based on cross-section images; colors are assigned based on marker expression (red: *Shh*; yellow: *nkx2.2a*; green: *mnx1*; blue: *gata2*). Part of the notochord (NC, *Shh*+) is included. (i) Morphogenesis during the patterning process; single cells can be tracked throughout (e.g., highlighted cell with red membrane). Tracks carry information of reporter expression (ii), lineage relationships (iii), and movement trajectories (iv). See also Figure S1A.

(E) Cross-sectional view (dorsal side up) of sample data set. Red indicates nuclei. A GFP+ stripe domain emerges (bracket, bottom-left image). Arrow points to differentiating MNs exiting the GFP domain. Scale bar, 10 μm. See also Movie S2.

(F) Relative speed of cell movement during neural tube formation. Each purple mark represents the speed of a single cell; 41 tracked ventral cells are plotted. Relative speed is calculated by dividing a cell's positional change (μm) between two time points over the time difference (11.5 min). Position is measured relative to the average position of all tracked cells to eliminate global movements introduced by embryo rotation/shifting. Orange marks show average speed. See also Figure S1F.

across different neural plate/tube morphologies, we measured cell positions and reporter intensities by GoFigure 2 (Figures S2A–S2E). The quantification (Figures 2C and 2C′) confirms direct observations from images and further indicates that at 10 hpf, the Shh response gradient is heterogeneous, broad, and almost flat over a 60 μm range. It gradually becomes steeper and less heterogeneous over time as Kaede levels increase in the 30 μm range and drop beyond. These data show that each position has a different temporal Shh response profile that is further varied due to local heterogeneity, likely modulated by the movement of both source and responding cells. Together, our observations pose a challenge to the positional specification model where conceptually, a static progenitor field and a smooth morphogen gradient are required for precise pattern formation. How do neural progenitors get patterned correctly into "stripes" (Figures 1E and S1A) when neither a static field nor a smooth gradient exists?

Progenitors Make Early Fate Decisions in Wide and Overlapping Ranges

To characterize the spatial distribution and timing of specification of the progenitors, we tracked the motor neuron progenitors

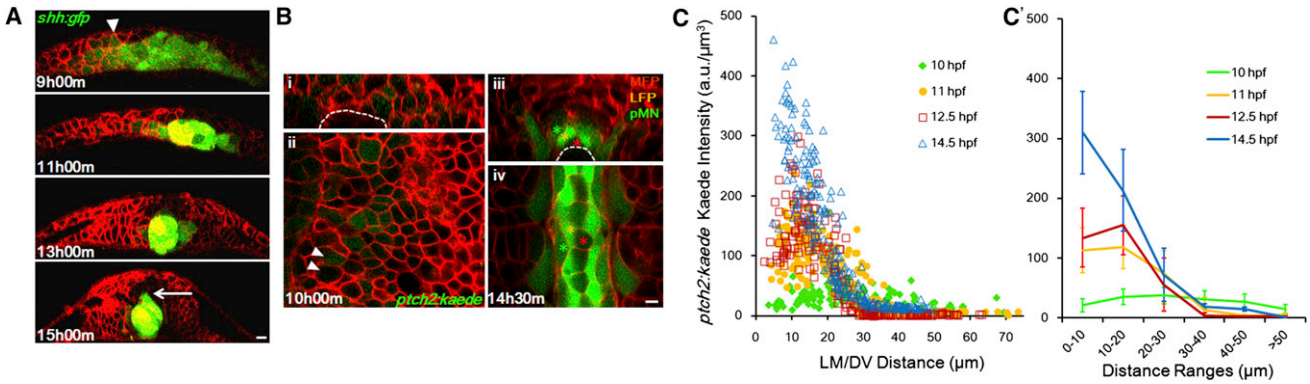

Figure 2. Shape Changes of Shh Gradient and Heterogeneity in Spatial Distribution of Responses

(A) Time course of notochord formation by *shh:gfp*+ cells in cross-section. Red shows mem-mCherry (same below). Arrowhead points to GFP+ cells in neural ectoderm/plate. Arrow indicates MFP cell expressing GFP. Scale bar, 10 μm.

(B) Cross-section (i and iii) and longitudinal section (ii and iv) of *ptch2:kaede* expression pattern. Arrowheads point to neighbor cells with different Kaede levels. Asterisks indicate stereotypic cell fates at the indicated locations. Scale bar, 10 μm. See also Figure S1A.

(C and C′) Kaede level spatial distribution through time. Each mark represents a segmented cell with measured position and fluorescence intensity. (C′) is a spatially averaged (±SD) representation of (C). Kaede intensities in the notochord cells were subtracted as background.

(pMNs) and the lateral floor plate cells (LFPs), using *mnx1:gfp*, *olig2:gfp*, and *nkx2.2a:mgfp* expression to distinguish their fates (Jessen et al., 1998; Shin et al., 2003; Flanagan-Steet et al., 2005; Figure S1A). Previous studies have detected pMN and LFP marker expressions before 12 hpf (Korzh et al., 1993; Schäfer et al., 2005), suggesting early specification in the neural plate stages. To capture the earliest *mnx1:gfp*+ cells, we performed imaging without other fluorescent cell markers (Figure 3A). Scattered GFP+ cells can be found shortly after 10.5 hpf, followed by more in a wide LM range, and interestingly, intermingled with GFP− cells. In trackable data sets where ubiquitous cell markers are used, *mnx1:gfp*+ cells can only be distinguished later (13 hpf) because of bleed-through signal, but importantly, these tracks show that GFP levels increase monotonically, and LFP cells do not turn on GFP (Figure 3B). Moreover, this GFP increase is unaffected by Shh inhibitor Cyclopamine (Figure S3A), suggesting independence of GFP expression from further Shh signaling. These data indicate that the onset of *mnx1:gfp* marks actual fate specification to pMNs instead of LFPs. To further assess timing of pMN specification, we performed a time course treatment of Cyclopamine and counted MN numbers from treated embryos (Figures 3C and S3B). Early blockade (before 12 hpf) of Shh activity greatly reduces MNs, whereas later treatment causes a milder reduction, suggesting that a significant portion of pMNs is specified early.

Olig2 reporter marks the dorsal boundary of pMN domain in the final pattern (Figure S1A). Similar to the *mnx1:gfp*+ cells, *olig2:gfp*+ cells emerge at different positions with negative and positive cells intermingled in a "salt-and-pepper" fashion, most evidently dorsal-laterally (Figure 3D). GFP quantification shows that the olig2 "stripe" arises from a mixed population over a wide range (Figure 3E). Nkx2.2a reporter marks the LFP domain and borders *mnx1:gfp* expression ventrally (Figure S1A). *Nkx2.2a:mgfp*+ cells start to be detectable around 13 hpf at variable locations but become restricted to the stereotypic two columns on both sides of the MFP cell after 15 hpf (Figure S3C). The distribution of LFPs is wide initially and becomes narrower (Figure S3D), suggesting that the LFP domain also arises from mixed populations, although not as evident as pMNs, likely due to the small size (two cells) of the LFP stripe.

Together, these data suggest that specification of ventral progenitors occurs early in spatially mixed distributions, not in sharply segregated stripes. These stripes form later in the final pattern. However, because tracking of transgenic marker expression is challenging at earlier times, it remains possible that progenitors only transiently express these markers and then either repress or increase the expression depending on the Shh level at their positions (Dessaud et al., 2010). In this scenario, early heterogeneity in the Shh gradient would be irrelevant because the progenitors remain labile, and the early erroneous responses would be overwritten by an improved gradient (Figure 3F, i). Alternatively, it is possible that the early response is maintained, and these specified cells physically move into the locations that match their specified identity (Figure 3F, ii).

Progenitor Divisions Are Lineage Restricted and Contribute to Cell Mixing

To further refine our estimate of the timing of cell specification, we analyzed the lineage trees of identified progenitors. By tracking the mothers and/or grandmothers of specified cells back to as early as neural ectoderm stages, we found, strikingly, a strong positive correlation of fate in sister and first cousin cells in the pMN and LFP pools (Figure 4A). We did not observe any divisions that generate a pMN and a LFP cell (0 out of 83); more generally, the final divisions rarely lead to two progenitors of different types. Because a great portion of these divisions (30 out of 83) happen before 12 hpf (Figure S4A), these results argue against the labile cell fate idea because sister cells adopting different progenitor fates should be found if specification happens late, unless sister cells keep sharing the same position in the Shh gradient (e.g., they are neighbors). To test this, we followed the positional dynamics of sister cells in pairs by

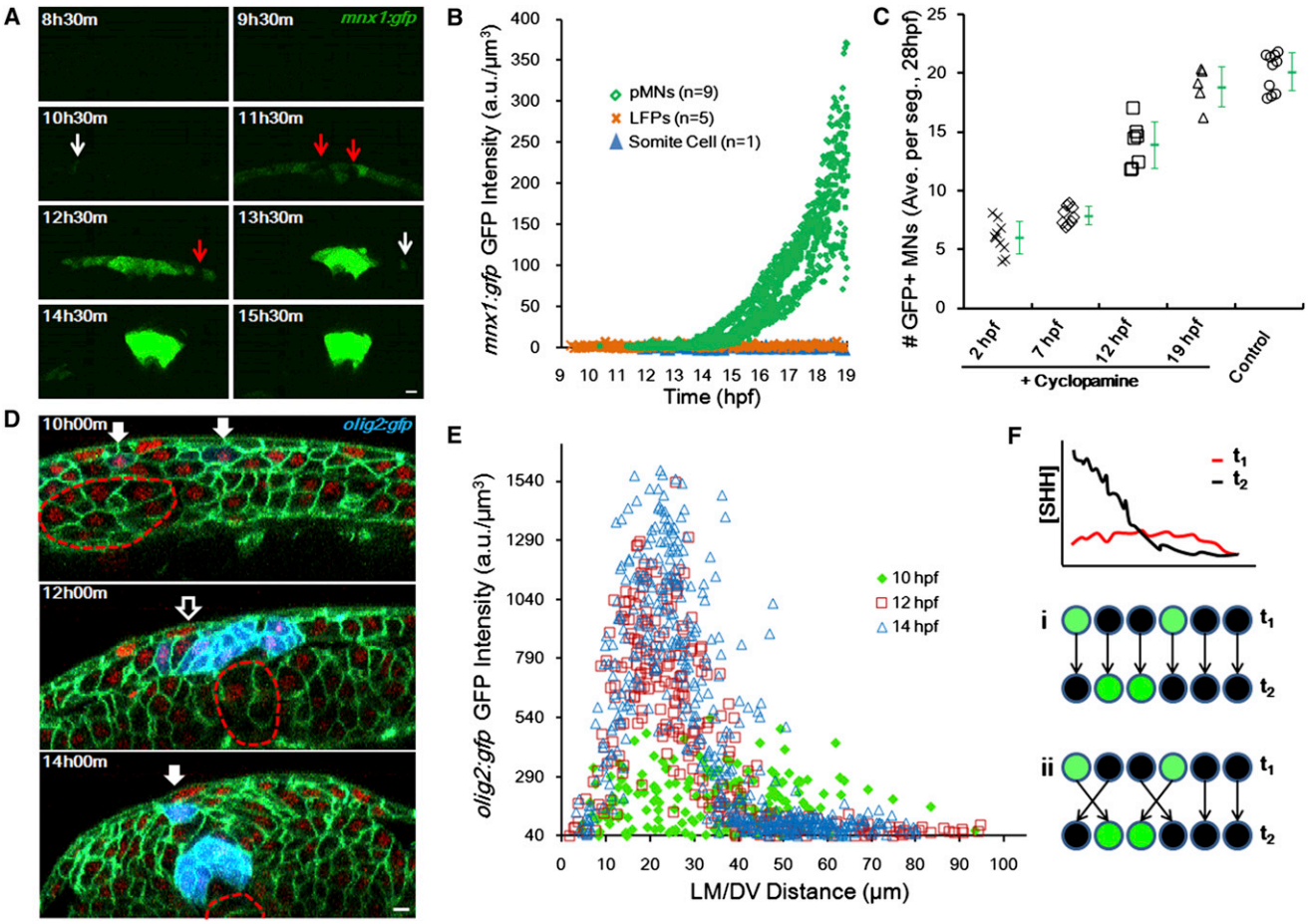

Figure 3. Progenitor Fates Are Specified during Cell Movements in Mixed Distributions

(A) Time course of *mnx1:gfp* expression. Images are cross-sectional examples. Red arrows point to mixed negative cells. White arrows indicate scattered positive cells. Scale bar, 10 μm.

(B) GFP (*mnx1:gfp*) levels in tracked cells through time. See also Figure S3A.

(C) Time course of Cyclopamine inhibition of pMN specification. Treatment of 100 μM Cyclopamine started at indicated times, and MNs were counted at 28 hpf as an indicator of pMN number. Numbers are averaged per embryo by number of neural segments counted. Green marks show average (±SD). See also Figure S3B.

(D) *olig2:gfp* (blue) domain formation. Green indicates cell membrane. Red shows cell nucleus. Filled arrows point to scattered positive cells. Empty arrows indicate mixed negative cells. Dashed lines represent notochord boundary. Scale bar, 10 μm.

(E) Spatial distribution of *olig2:gfp*+ cells. At 10 hpf, they scatter in a wider range and are mixed with negative cells; in contrast, at 14 hpf, positive cells form a major stripe between 15 and 30 μm where negative cells are absent.

(F) Two models for sharp stripe formation. (i) Late (improved) gradient rewrites responses, predicting late specification and stable positions. (ii) Cell sorting corrects wrong positions, predicting early specification and rearrangement afterward.

measuring their separation distance over time (Figure 4B). We found that daughter cells immediately become separated after cell division, even if they become neighbors later, suggesting that cell division is one cause of positional mixing. Daughter cells of the same fate can be found on opposite sides of the midline and in different segments of the neural tube (Figure S4B), consistent with previous studies by Kimmel et al. (1994) and Park et al. (2004). To determine whether these divisions might lead to a difference in sister cell positions in the Shh gradient, we analyzed 50 divisions throughout the LM/DV axis and time (Figures 4C and S4C). A significant portion (18 out of 50) of divisions happens along the LM/DV axis, so that the positions of the daughter cells relative to the notochord are clearly different. Together, these data show that sister cells share fate but not position at early stages of patterning, suggesting that specification (or at least fate bias) has been established in the mother/grandmother cells in a spatially mixed pattern within a dynamic tissue.

Our marker-tracking and lineage-tracing results show that cells may become specified at ''wrong'' places due to movements, divisions, and heterogeneous signaling. Additional mechanisms are required to make clean stripes from a dynamic, mixed progenitor population. Although up to this point cell movement appears to act as a limitation to morphogen-patterning precision, could the movements after specification contribute positively to the pattern (Figure 3F, ii)?

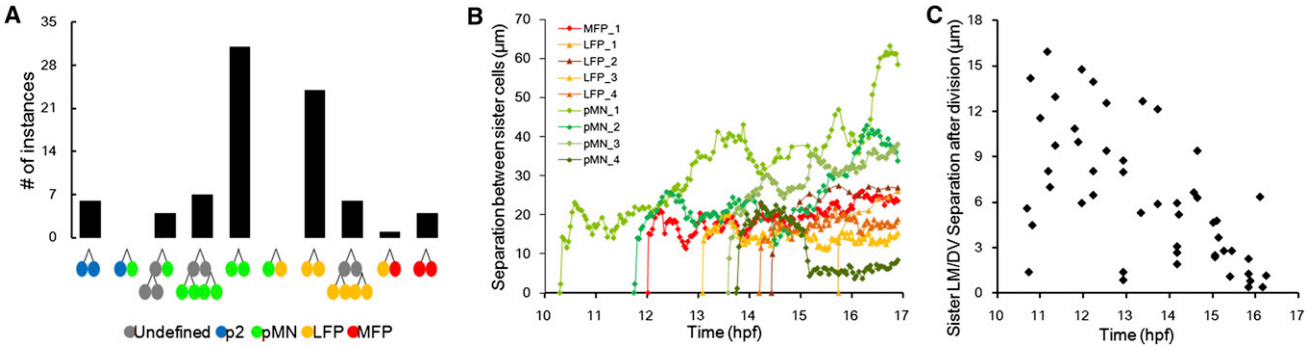

Figure 4. Progenitors Share Fate but Not Position with Sisters and Cousins at Early Stages

(A) Summary of lineage motif counts (n = 83). Counts are collected from 18 independent data sets. Motifs with two generations are not often captured in the imaged time window, so the count does not suggest that two-generation motifs happen in lower frequencies than one-generation motifs. Division times are before 12 hpf (n = 30), 12–14 hpf (n = 20), and after 14 hpf (n = 33). See also Figure S4A.

(B) Separation dynamics of sister cells after birth. The zero (0) points indicate the birth time of sister cells from division of the mother cell. A distance of 6–8 μm indicates that the sisters remain neighbors, 10–16 μm one cell separation, etc. See also Figure S4B.

(C) Cell divisions causing position instability. A total of 50 division events were randomly picked through time. A total of 18 divisions happened closely along the LM/DV axis, generating at least one-cell-diameter difference (>8 μm) in position between sister cells. At later time, more divisions are perpendicular to the LM/DV axis, generating no significant positional difference between sisters (<3 μm). See also Figure S4C.

Cell Sorting Establishes Sharply Bordered Progenitor Domains

To understand how cell movements contribute to patterning, we tracked cell-type-identified cells back in time. Surprisingly, we found that the early distribution of the progenitors does not match their final distribution in terms of relative position or order (Figures 5A and 5B). In this fully tracked ventral neural segment, progenitors that make the pattern (Figure 5A, iii and iv) are initially spread out and mixed with cells that will not join this segment (Figure 5A, i and ii). Moreover, future pMNs may start off either touching the notochord or located far away from the notochord. Later, all these pMNs come together to locate into a sharply bordered domain (Figure 5A). LFPs and MFPs also show similar behavior, albeit in smaller spatial ranges compared to pMNs (Figures 5B and S5A). The early distributions of tracked MFPs, LFPs, and pMNs resemble the wide and mixed patterns of early *shh:gfp*, *nkx2.2a:mgfp*, and *mnx1:gfp* expression, respectively (Figures 2A, S3C, and 3A). Although we found that the MFPs always touch the notochord and line up along the midline earliest (Figures 5B and 5C), pMNs and LFPs frequently intermingle and switch positions (Figures 5B and 5D; Movie S5). These rearrangements happen most often as cells enter the neural keel and after divisions. For example, in Movie S5, at 11 hpf, a LFP progenitor was initially located more lateral to a pMN in the neural plate. The LFP progenitor migrated dorsal to the pMN at around 12 hpf and remained no closer to the notochord than the pMN. It divided around 13 hpf, generating two future LFPs. As a result of this division, one daughter LFP was further dorsal compared to the pMN until around 14 hpf, when it moved to equal distances. Finally, after 14.5 hpf, this daughter LFP inserted between an MFP and the pMN and maintained that position onward. By locating the tracked cells in fully segmented neural plate/tube at different times (Figure 5E), we found that the pMN/LFP boundary marked by *mnx1:gfp* expression starts to emerge between tracked cells after 14.5 hpf; at times earlier than this, the pMNs and LFPs are located in wide ranges that overlap. Most ventral cells settle into stable positions by 15 hpf (Figure 5B). We verified cell fates by tracking with additional fate markers and determined that these cells stay stably within their domains by later-stage movies (Figures S5B–S5D; Movie S6; data not shown). These data demonstrate that cell sorting directly establishes the French flag pattern. The fact that cells at initially widely separated locations can have the same fate and final location whereas initial neighbors may have different final locations and fates is unexpected. This observation is inconsistent with the positional specification model. However, we note that on the population level, a rough correlation between position and fate exists throughout and is sharpened over time by cell sorting (Figure 5B, inset). Together, our data rule out the notion that naive cells are specified between spatial thresholds and remain in the same relative positions; instead, the progenitor domains and their boundaries form by sorting of specified cells from widely dispersed locations.

Our results suggest that cell sorting is required for pattern formation in the neural tube. To test this hypothesis, we mosaically perturbed cadherin-2 (cdh2), a neural adhesion molecule expressed by all neural progenitors and required for their movements, using a cdh2 morpholino and a dominant-negative version of cdh2 (Lele et al., 2002; Rieger et al., 2009). In the perturbed embryos, many *mnx1:gfp*+ cells are misplaced in a wider and more mixed pattern at stages by which stripes have formed in controls (Figures 5F, 5G, and S5E). Live imaging of perturbed cells reveals that their misplacement resulted from reduced integration into the neural keel/tube, which likely blocked cell sorting and thus preserved the noisy spatial pattern of specification (Movie S7). These data indicate that proper adhesion is required for cell sorting and, consequently, pattern formation.

Ectopically Induced pMNs Migrate to Form a Sharp Domain

A model in which pattern forms by sorting of specified cells predicts that ectopically induced progenitors should migrate to the

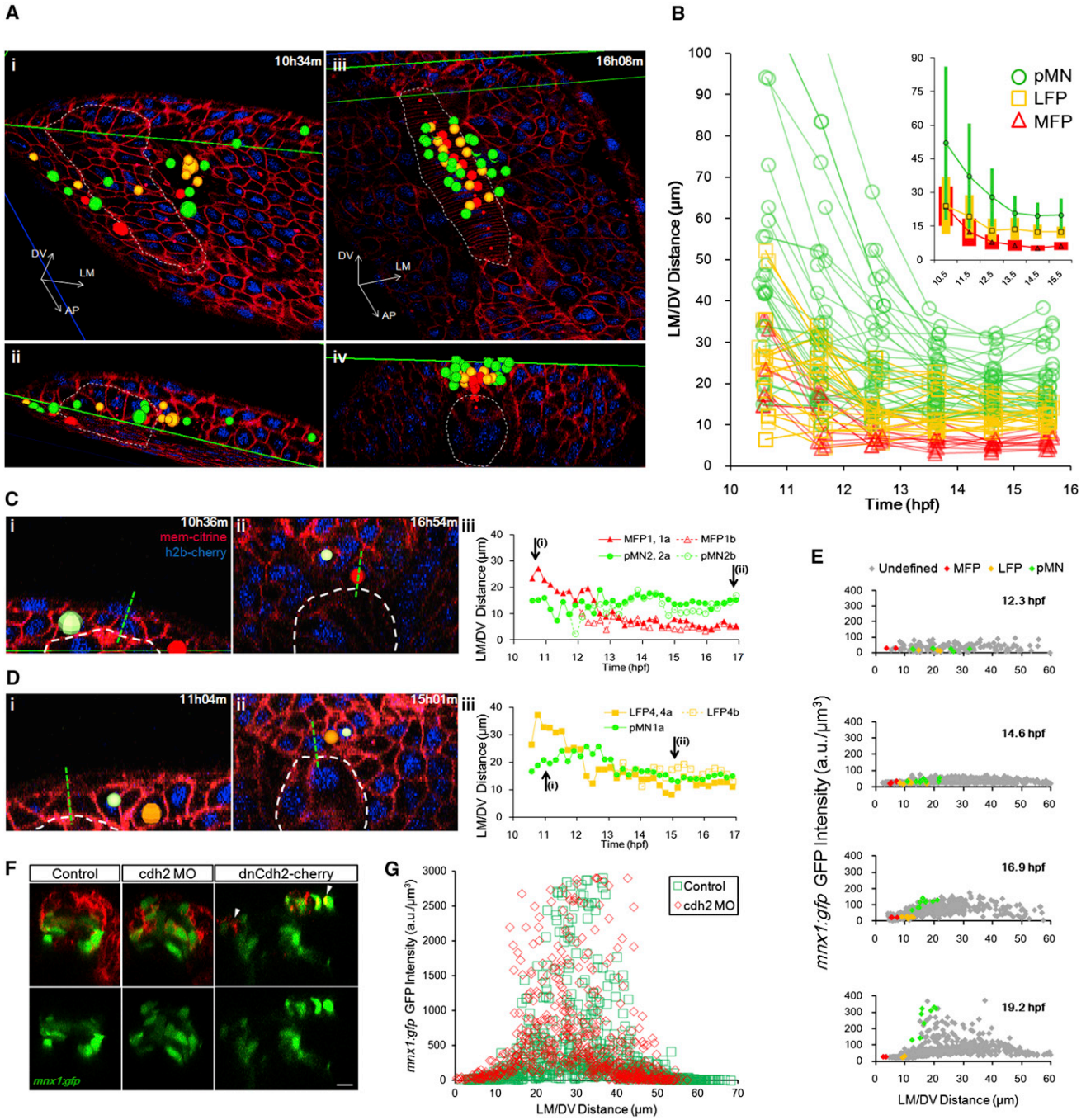

Figure 5. Progenitors Enter Stable Locations and Form Sharp Boundaries by Intensive Cell Rearrangement

(A) Distribution of tracked cells from a fully analyzed ventral neural segment (comprised of 7 MFPs, 13 LFPs, and >20 pMNs) at early neural plate stage (i and ii) and neural tube stage (iii and iv). (ii) and (iv) are corresponding cross-sectional views of (i) and (iii). Green lines indicate the intersection of cross-section view and dorsal view (i, ii, and lower line in iii) or the upper boundary of the data set (iv and upper line in iii). Colored spheres are 3D locations of tracked cells (red: MFP; orange: LFP; green: pMN). Dashed lines represent notochord boundary. Small red spheres are notochord top midline.

(B) Trajectories of tracked cells along the LM/DV axis demonstrating intensive sorting. For simplicity, only six time points on the tracks are plotted. A total of 66 tracks collected from four data sets are plotted. Some cells exhibit rearrangements beyond 16 hpf. Inset shows population average position ± SD (colored bars) of tracks by cell type plotted on the same axes. See also Figure S5A.

(C) Example of relative positional changes of a pMN (light green indicates pMN2a) and a MFP (red shows MFP1,1a). Green dashed line represents midline. White dashed line designates notochord boundary. (iii) Full movement trajectories of the cells (same in D; for simplicity, one of the daughter cell tracks is continued with the mother track).

(D) Example of positional switch between a pMN (light green indicates pMN1a) and a LFP cell (orange shows LFP4,4a). See also Movie S5.

(legend continued on next page)

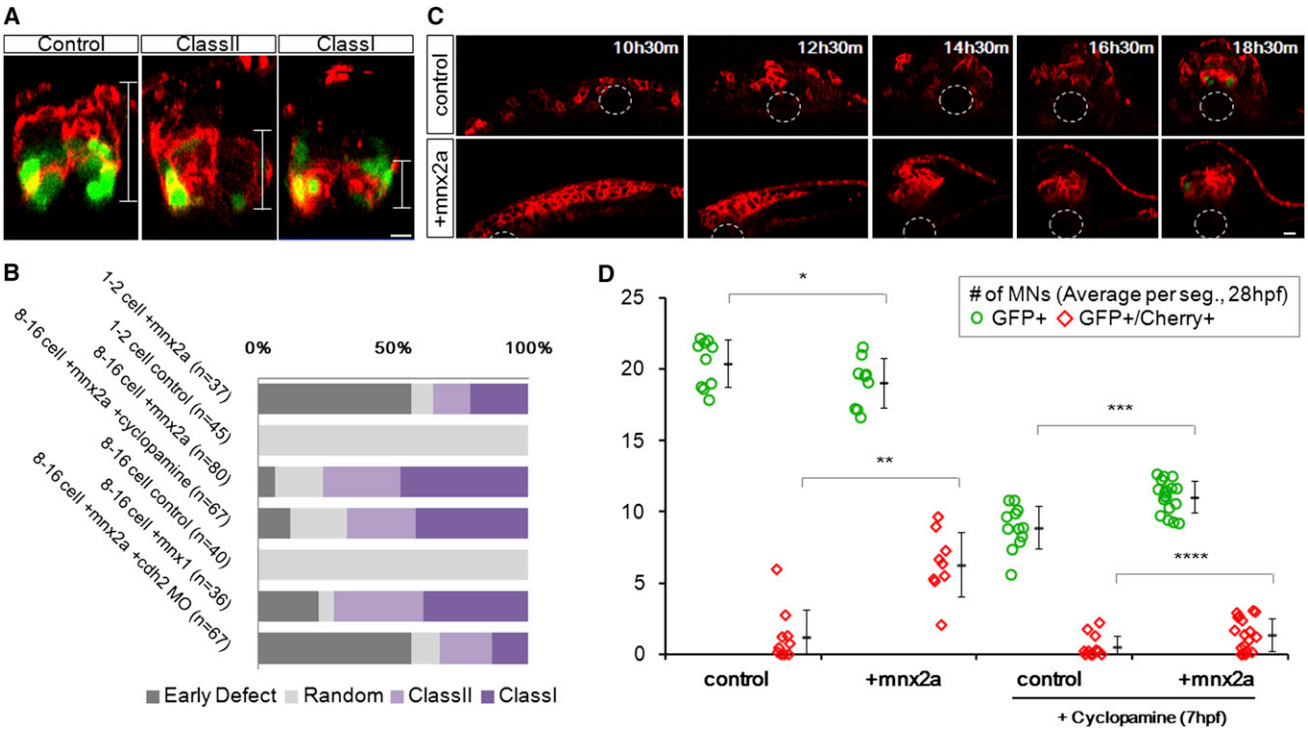

Figure 6. Ectopic Mnx2a-Expressing Cells Form a Sharp Ventral Domain Similar to the pMN Domain

(A) The 24 hpf neural tube phenotypes after injection of *mem-mCherry* ± *mnx2a* mRNAs in one blastomere at 8- to 16-cell stage are shown. Phenotypes are classified according to the distribution of mCherry+ cells (brackets): class I embryos contain cells only in the ventral third of the neural tube, class II embryos contain cells in the ventral two-thirds, and "random" contains injected cells throughout. Green indicates *mnx1:gfp*. Scale bars, 10 μm. See also Figure S6A.

(B) Summary of mosaic injection experiments. Early defect embryos failed to form neurula. Cyclopamine treatment started at 7 hpf.

(C) Sample time course of Mnx2a domain formation. This Mnx2a embryo became class II type. Dashed-line circles indicate position of the notochord. Green shows *mnx1:gfp*. Red designates mem-mCherry. Scale bar, 10 μm. See also Figure S6B.

(D) Mnx2a-expressing cells replace "normal" pMNs. Imaging and counting of MNs as Figure 3C. *p = 0.09, **p = 0.00004, ***p = 0.0001, and ****p = 0.03 (Student's t test).

correct positions corresponding to their fates. To test this prediction, we mosaically overexpressed the transcription factor Mnx2a, which is a marker of pMN (Wendik et al., 2004) and whose homolog MNR2 induces ectopic MNs in chick embryos (Tanabe et al., 1998). We injected *mnx2a* mRNA mixed with *mCherry* mRNA into one blastomere at the 8- to 16-cell stage. Strikingly, we found strong ventral segregation of mCherry-labeled cells to the normal pMN domain in *mnx2a*-injected embryos, whereas control embryos showed a random distribution of labeled cells across the DV axis (Figures 6A and 6B). In class I embryos, the pMN domain is fully occupied by descendants of the injected blastomere, and motor axons are strongly labeled evenly along the body axis (Figure S6A), a phenomenon never observed in control injections. Conversely, in the dorsal domains of the neural tube, in contrast to control embryos, injected cells are missing in *mnx2a*-injected embryos (Figures S6A and S6B). Mosaic overexpression of Mnx1 resulted in a similar phenotype (Figure 6B; data not shown). Quantification of GFP+ MNs further confirms that Mnx2a-injected cells contribute more extensively to the pMN domain as compared to random contribution of control *mCherry*-injected cells (Figure 6D). Cyclopamine treatment of injected embryos starting at 7 hpf does not alter the Mnx2a phenotypes (Figures 6B and S6C), suggesting that the ventral localization of Mnx2a-injected cells is independent of Shh response. Indeed, early-specified normal pMNs also form a smaller but sharp domain in the presence of Cyclopamine (Figure S3B). Mnx2a injection alleviates reduction of MNs by Cyclopamine treatment, and the injected cells express pMN markers and maintain progenitor location and morphology (Figures 6D and S6D), confirming that they have become specified to pMNs. To understand how the Mnx2a phenotypes arise at the cellular level, we tracked the

(E) *mnx1:gfp* expression boundary formation between LFPs and pMNs. GFP intensity distribution by position plotted for four time points. Each mark represents a cell (>200 cells per time point). Colored marks show tracked cells with known fates; gray marks indicate other segmented cells at the plotted time point.

(F) Cdh2 perturbations on *mnx1:gfp*+ domain formation. Images are 24 hpf cross-sections of mosaic-labeled (cherry ± cdh2 morpholino [MO] and dominant-negative Cdh2-cherry fusion [dnCdh2-cherry]) neural tubes. Arrowheads point to puncta of dnCdh2-cherry. Scale bar, 10 μm. See also Figure S5E and Movie S7.

(G) Quantification of GFP+ cell distribution in Cdh2 morphant and control. See also Figure S5E.

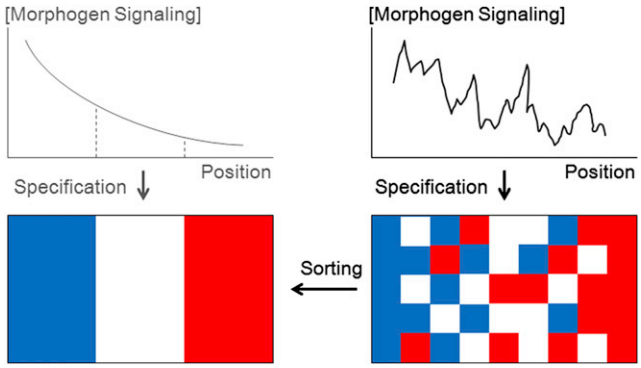

Figure 7. Revised French Flag Model Incorporating Dynamics of Morphogen Gradient and Cell Sorting

This model depicts specification and sorting sequentially for conceptual clarity, but they occur at different and overlapping times for different cells. See Discussion. See also Figure S7.

movement of injected cells. Interestingly, these cells form clusters in the early neural plate (Figure S6E; data not shown), suggesting adhesion changes accompanying specification. They migrate together to populate the ventral domains (Figure 6C) to give rise to Mnx2a phenotypes, and their ventral bias becomes evident after intercalating into the neural keel (Figure 6C, compare 14.5 and 16.5 hpf), similar to normal pMNs. These data suggest that Mnx2a may control specific adhesion affinities of pMNs that control their sorting. Indeed, in cdh2 morpholino and Mnx2a-coinjected embryos, despite severe disruption of morphogenesis, the injected cells remain colocalized and ventrally biased (Figures 6B and S6F).

Our results show that induced ectopic progenitors move to form sharp domains similar to the normal pattern in a Shh signaling-independent manner. They further suggest that specification creates adhesive differences between cells of different fates. Together, these data support a model in which specified progenitors self-assemble into precise spatial domains by cell adhesion-dependent cell sorting.

DISCUSSION

The Role of Cell Movement in Neural Plate/Tube Patterning

We captured a 4D picture of pattern formation from early neural plate to neural tube at single-cell, trackable resolution in zebrafish and discovered that the sharply delineated pattern of progenitor domains forms through sorting of specified cells. Our observations challenge and extend the classic positional specification model in several ways. First, the classic model assumes graded response as a function of position in a smooth, monotonic morphogen gradient. Although we do not know how closely the distribution of Shh molecules in the neural plate resembles such a gradient, we have shown that the response is highly dynamic and heterogeneous. We suggest that, even if Shh morphogen forms a perfect gradient, the movements of the cells will inevitably complicate their Shh exposure, making the response pattern noisy. Second, the classic model suggests that naive cells become specified at stereotypic positions. We have shown that fate markers are expressed in intermingled patterns during and preceding more cell movements. In addition, cell fates are lineage restricted (e.g., pMN versus LFP) long before the final pattern emerges. These observations indicate that specification and positioning are separate in time, and cells get specified outside stereotypic positions. Third, the classic model interprets the ventral-to-dorsal-progressing pattern of Shh-mediated gene expression (Jeong and McMahon, 2005) as a result of stationary cells changing their gene expression as they accumulate more Shh signals (Chamberlain et al., 2008; Dessaud et al., 2010). Our observations suggest that, in addition to gene expression changes, cells can maintain their gene expression state and physically move to contribute to the refining pattern (e.g., a pMN moves away from the notochord). Together, we propose a revised model for neural tube patterning incorporating imprecision of positional information and cell movement (Figures 7 and S7). Cell positions are unstable in the dynamic tissue, and morphogen signaling across the tissue is spatially noisy (at least in part due to movement of responding cells), resulting in a salt-and-pepper specification pattern. Cell sorting then segregates different progenitors into sharply defined domains.

Although important for neural tube patterning in zebrafish, the role of cell movement in other vertebrates such as chick and mice remains to be elucidated and may be different or context dependent. The modes of neural tube morphogenesis among vertebrates vary considerably presumably depending on the degree of progenitor epithelialization (Smith and Schoenwolf, 1997; Clarke, 2009). For example, in primary neurulation that occurs in the anterior neural tubes of chick and mice, an epithelialized cell sheet undergoes a folding process that forms a lumen through invagination (Smith and Schoenwolf, 1997). In secondary neurulation that occurs more posteriorly, however, a neural rod of less-epithelialized cells forms first that then cavitates to form a lumen de novo as cells epithelialize (Catala et al., 1996). We have observed that more epithelialized cells have less mobility in zebrafish. The higher degree of epithelialization in primary neurulation suggests that there is unlikely as much cell mixing or rearrangement as in the zebrafish neural tube, which shares more similarities with secondary neurulation (Clarke, 2009). The amount of cell movement in chick and mice neural tubes has been assessed by clonal-labeling studies (Leber and Sanes, 1995; Inoue et al., 2000; Das and Storey, 2012). These studies show that there is wide cell dispersion at early stages but little cell movement later. Unfortunately, the exact trajectories of these cell movements, times of cell divisions, and how they relate to Shh responses and specification are not clear. To determine to what extent (if any) cell sorting contributes to neural tube patterning in these vertebrates, imaging data comparable to ours in spatial temporal resolution and coverage are required. We note that ongoing efforts toward these goals show promising potential (Yamaguchi et al., 2011; Das and Storey, 2012).

The Mechanisms Controlling Cell Sorting

We have not yet determined the molecular details of cell sorting, but our data suggest that it is a complex process likely orchestrated by multiple adhesion molecules. We have shown that

Cdh2 is required for proper pMN domain formation. In addition, Mnx2a appears to cause adhesion changes that drive sorting of ectopic pMNs, suggesting that specification downstream of Shh signaling may activate fate-specific affinities, as observed in the abdomen of *Drosophila* (Lawrence et al., 1999). In our movies, we also found that cell rearrangements happen most often as cells mix during intercalation while forming the neural keel and after divisions, conditions that likely facilitate the effect of short-ranged adhesion forces. Disruption of such intercalation results in misplaced progenitors. Previously, it has been shown that differential adhesion can mediate migration and pool sorting of postmitotic neurons (Price et al., 2002), a process that follows progenitor domain formation. A similar strategy might be employed by the progenitors because they also express different cadherins and protocadherins in conserved patterns along the DV axis (Lin et al., 2012). What sets of specific adhesion molecules correspond to different progenitor fates and how they are regulated and cooperate to control cell sorting remain to be elucidated.

An alternative sorting mechanism is chemotaxis of specified cells, in which the direction and final location of sorting are determined by diffusible signals, whereas adhesion molecules only serve as the structural necessity for cells to move. We have shown that Shh response is not required for sorting, but it remains possible that noncanonical Shh or other molecular gradients (e.g., Bmp, Wnt) provide positional cues for cell movement.

Cell Self-Assembly Confers Robustness to Positional Noise and Errors

The formation of spatially distinct domains faces noise at multiple scales, including molecular noise as described previously by Paulsson (2004) and Lander et al. (2009), and cell positional noise caused by cell movements as described here. We believe that multiple strategies are used to achieve robust patterning in the face of this noise. The intracellular GRN (Balaskas et al., 2012) can help make and maintain correct fate decisions by canalizing noisy signaling inputs into discrete, nonoverlapping states of gene expression and thus cell fates. Intercellular interactions, such as cell sorting shown in this study, allow overlapping distributions of cell types caused by spatially noisy signaling to be corrected. Furthermore, other intercellular interactions such as lateral inhibition may play a role in size control of progenitor domains. For example, in Mnx2a-injected embryos, the final number of pMNs seems to be regulated despite being initially too large, suggesting that ectopic Mnx2a-expressing cells may prevent uninjected cells from becoming pMNs. Characterizing the molecular and cellular details of these different interactions will be vitally important for understanding how embryos canalize molecular and positional noise as well as genetic and environmental variation to attain developmental norms (Waddington, 1942).

In summary, our study highlights the power and importance of live observation of cell behavior in understanding developmental patterning and provides a model of how patterns robustly arise in the dynamic environment of the developing ventral neural tube. Cell sorting by differential affinities is a classical idea (Steinberg, 1963) alongside the morphogen model (Wolpert, 1969). There is no reason to think that Shh signaling is unique in showing a highly dynamic, noisy pattern of activity. If these are general features of morphogens, then self-assembly may be a general mechanism to assign positions to specified cells because cell movement is common during the morphogenesis and proliferation of both signaling centers and their target fields (Kay and Thompson, 2009).

EXPERIMENTAL PROCEDURES

Zebrafish Strains and Maintenance

See the Extended Experimental Procedures for protocols, sources, and references for transgenic strains used in this study. All fish-related procedures were carried out with the approval of Institutional Animal Care and Use Committee (IACUC) at Harvard University.

Microinjections of mRNAs

For in toto labeling, one-cell-stage embryos were injected (Nanoject) 2.3 nl 40 ng/μl of labeling mRNA(s) (h2b-cherry, mem-citrine, mem-cherry, mem-EBFP2, and combinations). For mosaic injections, one blastomere of 8- to 32-cell-stage embryos was injected with approximately 1 nl 20 ng/μl one labeling mRNA with or without 10 ng/μl *mnx2a, dnCdh2-cherry* mRNA.

Time-Lapse Two-Photon/Confocal Imaging

Live imaging was performed using a Zeiss 710 confocal/two-photon microscope (objective: C-Apochromat 40× 1.2 NA) with a homemade heating chamber maintaining 28°C. Chameleon (Coherent) laser line 1,020 nm was used for three-channel two-photon in toto sessions. See Figure S1 and the Extended Experimental Procedures for details.

Image Data Analysis

Nuclear segmentation and tracking were performed using GoFigure 2, an open-source, cross-platform software application we have developed for image analysis (http://www.gofigure2.org). Segmentation and track tables exported from GoFigure 2 were further processed and plotted with Microsoft Excel. See Figures S1 and S2 and the Extended Experimental Procedures for details.

SUPPLEMENTAL INFORMATION

Supplemental Information includes Extended Experimental Procedures, seven figures, and seven movies and can be found with this article online at http://dx.doi.org/10.1016/j.cell.2013.03.023.

ACKNOWLEDGMENTS

We thank D. D'India for fish care, H. Otsuna for movie making, R. Koster, D. Meyer, U. Strähle, B. Appel, S. Higashijima, S. Lin, and L. Zon for sharing reagents, D. Tulga and T. Hiscock for technical assistance, and Q. Mao, R. Noche, A. Green, Y. Chen, W. Ma, R. Ward, A. McMahon, M. Kirschner, C. Cepko, and T. Mitchison for comments. This work is supported by NIH grants HG004071 and DC010791. F.X. is also supported by the graduate program of Biological Sciences in Dental Medicine at Harvard University. F.X. and S.G.M. conceived this study. F.X., A.R.T., and P.H. performed the experiments. F.X. analyzed the data. A.G., K.R.M., L.S., and N.R. provided tools and assistance for data analysis. P.H., I.A.S., N.D.O., P.D.C, and A.F.S. provided reagents and technical assistance. F.X. and S.G.M. wrote the manuscript. All authors discussed the manuscript and contributed to writing.

Received: September 24, 2012
Revised: January 22, 2013
Accepted: March 13, 2013
Published: April 25, 2013

REFERENCES

Ahn, S., and Joyner, A.L. (2004). Dynamic changes in the response of cells to positive hedgehog signaling during mouse limb patterning. Cell *118*, 505–516.

Balaskas, N., Ribeiro, A., Panovska, J., Dessaud, E., Sasai, N., Page, K.M., Briscoe, J., and Ribes, V. (2012). Gene regulatory logic for reading the Sonic Hedgehog signaling gradient in the vertebrate neural tube. Cell *148*, 273–284.

Catala, M., Teillet, M.A., De Robertis, E.M., and Le Douarin, M.L. (1996). A spinal cord fate map in the avian embryo: while regressing, Hensen's node lays down the notochord and floor plate thus joining the spinal cord lateral walls. Development *122*, 2599–2610.

Chamberlain, C.E., Jeong, J., Guo, C., Allen, B.L., and McMahon, A.P. (2008). Notochord-derived Shh concentrates in close association with the apically positioned basal body in neural target cells and forms a dynamic gradient during neural patterning. Development *135*, 1097–1106.

Ciruna, B., Jenny, A., Lee, D., Mlodzik, M., and Schier, A.F. (2006). Planar cell polarity signalling couples cell division and morphogenesis during neurulation. Nature *439*, 220–224.

Clarke, J. (2009). Role of polarized cell divisions in zebrafish neural tube formation. Curr. Opin. Neurobiol. *19*, 134–138.

Das, R.M., and Storey, K.G. (2012). Mitotic spindle orientation can direct cell fate and bias Notch activity in chick neural tube. EMBO Rep. *13*, 1030.

Dessaud, E., Yang, L.L., Hill, K., Cox, B., Ulloa, F., Ribeiro, A., Mynett, A., Novitch, B.G., and Briscoe, J. (2007). Interpretation of the sonic hedgehog morphogen gradient by a temporal adaptation mechanism. Nature *450*, 717–720.

Dessaud, E., Ribes, V., Balaskas, N., Yang, L.L., Pierani, A., Kicheva, A., Novitch, B.G., Briscoe, J., and Sasai, N. (2010). Dynamic assignment and maintenance of positional identity in the ventral neural tube by the morphogen sonic hedgehog. PLoS Biol. *8*, e1000382.

Echelard, Y., Epstein, D.J., St-Jacques, B., Shen, L., Mohler, J., McMahon, J.A., and McMahon, A.P. (1993). Sonic hedgehog, a member of a family of putative signaling molecules, is implicated in the regulation of CNS polarity. Cell *75*, 1417–1430.

Ericson, J., Briscoe, J., Rashbass, P., van Heyningen, V., and Jessell, T.M. (1997). Graded sonic hedgehog signaling and the specification of cell fate in the ventral neural tube. Cold Spring Harb. Symp. Quant. Biol. *62*, 451–466.

Erskine, L., Patel, K., and Clarke, J.D. (1998). Progenitor dispersal and the origin of early neuronal phenotypes in the chick embryo spinal cord. Dev. Biol. *199*, 26–41.

Flanagan-Steet, H., Fox, M.A., Meyer, D., and Sanes, J.R. (2005). Neuromuscular synapses can form in vivo by incorporation of initially aneural postsynaptic specializations. Development *132*, 4471–4481.

Harfe, B.D., Scherz, P.J., Nissim, S., Tian, H., McMahon, A.P., and Tabin, C.J. (2004). Evidence for an expansion-based temporal Shh gradient in specifying vertebrate digit identities. Cell *118*, 517–528.

Huang, P., Xiong, F., Megason, S.G., and Schier, A.F. (2012). Attenuation of Notch and Hedgehog signaling is required for fate specification in the spinal cord. PLoS Genet. *8*, e1002762.

Inoue, T., Nakamura, S., and Osumi, N. (2000). Fate mapping of the mouse prosencephalic neural plate. Dev. Biol. *219*, 373–383.

Jeong, J., and McMahon, A.P. (2005). Growth and pattern of the mammalian neural tube are governed by partially overlapping feedback activities of the hedgehog antagonists patched 1 and Hhip1. Development *132*, 143–154.

Jessell, T.M. (2000). Neuronal specification in the spinal cord: inductive signals and transcriptional codes. Nat. Rev. Genet. *1*, 20–29.

Jessen, J.R., Meng, A., McFarlane, R.J., Paw, B.H., Zon, L.I., Smith, G.R., and Lin, S. (1998). Modification of bacterial artificial chromosomes through chi-stimulated homologous recombination and its application in zebrafish transgenesis. Proc. Natl. Acad. Sci. USA *95*, 5121–5126.

Kay, R.R., and Thompson, C.R. (2009). Forming patterns in development without morphogen gradients: scattered differentiation and sorting out. Cold Spring Harb. Perspect. Biol. *1*, a001503.

Kimmel, C.B., Warga, R.M., and Kane, D.A. (1994). Cell cycles and clonal strings during formation of the zebrafish central nervous system. Development *120*, 265–276.

Korzh, V., Edlund, T., and Thor, S. (1993). Zebrafish primary neurons initiate expression of the LIM homeodomain protein Isl-1 at the end of gastrulation. Development *118*, 417–425.

Krauss, S., Concordet, J.P., and Ingham, P.W. (1993). A functionally conserved homolog of the *Drosophila* segment polarity gene hh is expressed in tissues with polarizing activity in zebrafish embryos. Cell *75*, 1431–1444.

Lander, A.D., Lo, W.C., Nie, Q., and Wan, F.Y. (2009). The measure of success: constraints, objectives, and tradeoffs in morphogen-mediated patterning. Cold Spring Harb. Perspect. Biol. *1*, a002022.

Lawrence, P.A., Casal, J., and Struhl, G. (1999). The hedgehog morphogen and gradients of cell affinity in the abdomen of *Drosophila*. Development *126*, 2441–2449.

Leber, S.M., and Sanes, J.R. (1995). Migratory paths of neurons and glia in the embryonic chick spinal cord. J. Neurosci. *15*, 1236–1248.

Lek, M., Dias, J.M., Marklund, U., Uhde, C.W., Kurdija, S., Lei, Q., Sussel, L., Rubenstein, J.L., Matise, M.P., Arnold, H.H., et al. (2010). A homeodomain feedback circuit underlies step-function interpretation of a Shh morphogen gradient during ventral neural patterning. Development *137*, 4051–4060.

Lele, Z., Folchert, A., Concha, M., Rauch, G.J., Geisler, R., Rosa, F., Wilson, S.W., Hammerschmidt, M., and Bally-Cuif, L. (2002). parachute/n-cadherin is required for morphogenesis and maintained integrity of the zebrafish neural tube. Development *129*, 3281–3294.

Lewis, K.E., and Eisen, J.S. (2003). From cells to circuits: development of the zebrafish spinal cord. Prog. Neurobiol. *69*, 419–449.

Lin, J., Wang, C., and Redies, C. (2012). Expression of delta-protocadherins in the spinal cord of the chicken embryo. J. Comp. Neurol. *520*, 1509–1531.

Martí, E., Takada, R., Bumcrot, D.A., Sasaki, H., and McMahon, A.P. (1995). Distribution of Sonic hedgehog peptides in the developing chick and mouse embryo. Development *121*, 2537–2547.

Megason, S.G., and Fraser, S.E. (2003). Digitizing life at the level of the cell: high-performance laser-scanning microscopy and image analysis for in toto imaging of development. Mech. Dev. *120*, 1407–1420.

Mosaliganti, K.R., Noche, R.R., Xiong, F., Swinburne, I.A., and Megason, S.G. (2012). ACME: automated cell morphology extractor for comprehensive reconstruction of cell membranes. PLoS Comput. Biol. *8*, e1002780.

Nicol, A., Rappel, W., Levine, H., and Loomis, W.F. (1999). Cell-sorting in aggregates of Dictyostelium discoideum. J. Cell Sci. *112*, 3923–3929.

Park, H.C., Shin, J., and Appel, B. (2004). Spatial and temporal regulation of ventral spinal cord precursor specification by Hedgehog signaling. Development *131*, 5959–5969.

Paulsson, J. (2004). Summing up the noise in gene networks. Nature *427*, 415–418.

Price, S.R., De Marco Garcia, N.V., Ranscht, B., and Jessell, T.M. (2002). Regulation of motor neuron pool sorting by differential expression of type II cadherins. Cell *109*, 205–216.

Rieger, S., Senghaas, N., Walch, A., and Köster, R.W. (2009). Cadherin-2 controls directional chain migration of cerebellar granule neurons. PLoS Biol. *7*, e1000240.

Schäfer, M., Kinzel, D., Neuner, C., Schartl, M., Volff, J.N., and Winkler, C. (2005). Hedgehog and retinoid signalling confines nkx2.2b expression to the lateral floor plate of the zebrafish trunk. Mech. Dev. *122*, 43–56.

Schoenwolf, G.C. (1991). Cell movements driving neurulation in avian embryos. Development *2*(*Suppl 2*), 157–168.

Shin, J., Park, H.-C., Topczewska, J.M., Mawdsley, D.J., and Appel, B. (2003). Neural cell fate analysis in zebrafish using olig2 BAC transgenics. Methods Cell Sci. *25*, 7–14.

Shkumatava, A., Fischer, S., Müller, F., Strahle, U., and Neumann, C.J. (2004). Sonic hedgehog, secreted by amacrine cells, acts as a short-range signal to direct differentiation and lamination in the zebrafish retina. Development *131*, 3849–3858.

Smith, J.L., and Schoenwolf, G.C. (1997). Neurulation: coming to closure. Trends Neurosci. *20*, 510–517.

Steinberg, M.S. (1963). Reconstruction of tissues by dissociated cells. Some morphogenetic tissue movements and the sorting out of embryonic cells may have a common explanation. Science *141*, 401–408.

Sürmeli, G., Akay, T., Ippolito, G.C., Tucker, P.W., and Jessell, T.M. (2011). Patterns of spinal sensory-motor connectivity prescribed by a dorsoventral positional template. Cell *147*, 653–665.

Takamiya, M., and Campos-Ortega, J.A. (2006). Hedgehog signalling controls zebrafish neural keel morphogenesis via its level-dependent effects on neurogenesis. Dev. Dyn. *235*, 978–997.

Tanabe, Y., William, C., and Jessell, T.M. (1998). Specification of motor neuron identity by the MNR2 homeodomain protein. Cell *95*, 67–80.

Waddington, C.H. (1942). The canalization of development and the inheritance of acquired characteristics. Nature *150*, 563–565.

Wendik, B., Maier, E., and Meyer, D. (2004). Zebrafish mnx genes in endocrine and exocrine pancreas formation. Dev. Biol. *268*, 372–383.

Wolpert, L. (1969). Positional information and the spatial pattern of cellular differentiation. J. Theor. Biol. *25*, 1–47.

Xu, Q., Mellitzer, G., Robinson, V., and Wilkinson, D.G. (1999). In vivo cell sorting in complementary segmental domains mediated by Eph receptors and ephrins. Nature *399*, 267–271.

Yamada, T., Pfaff, S.L., Edlund, T., and Jessell, T.M. (1993). Control of cell pattern in the neural tube: motor neuron induction by diffusible factors from notochord and floor plate. Cell *73*, 673–686.

Yamaguchi, Y., Shinotsuka, N., Nonomura, K., Takemoto, K., Kuida, K., Yosida, H., and Miura, M. (2011). Live imaging of apoptosis in a novel transgenic mouse highlights its role in neural tube closure. J. Cell Biol. *195*, 1047–1060.